Monthly Notices
of the
ROYAL ASTRONOMICAL SOCIETY

Mon. Not. R. Astron. Soc. **422,** 1109–1121 (2012) doi:10.1111/j.1365-2966.2012.20684.x

The star field age–metallicity relationship of the Small Magellanic Cloud

Andrés E. Piatti★

Instituto de Astronomía y Física del Espacio, CC 67, Suc. 28, 1428 Ciudad de Buenos Aires, Argentina

Accepted 2012 February 2. Received 2012 January 31; in original form 2011 September 8

ABSTRACT

We present the results of the age and metallicity estimates for the unprecedented data base of some 3.3 million stars distributed throughout the entire Small Magellanic Cloud main body, obtained for the first time from CCD Washington CT_1 photometry. We produce the first comprehensive star field age–metallicity relationship (AMR) from the birth of the galaxy until ∼1 Gyr ago, independent of any other previous approach. We find that the field stars do not possess gradients in age and metallicity, and that stellar populations formed since ∼2 Gyr ago are more metal rich than [Fe/H] ~ -0.8 dex and are confined to the innermost region (semi-major axis $\lesssim 1^\circ$). For the first time, we compare, homogeneously, the present star field AMR to that of the star cluster population with ages and metallicities in the same star field scales, and find that clusters and star fields share similar chemical evolution histories. Both galaxy components have experienced two enhanced formation processes: the most recent peaked at an age of ∼2 Gyr, and an earlier one detected at an age of ∼5–6 and 7.5 Gyr for clusters and star fields, respectively.

Key words: techniques: photometric – Magellanic Clouds – galaxies: individual: Small Magellanic Cloud – galaxies: star clusters: general.

1 INTRODUCTION

The study of the age–metallicity relationship (AMR) of Small Magellanic Cloud (SMC) star fields has been the subject of an exciting debate. Since Harris & Zaritsky (2004, hereafter HZ04) presented the first-ever global spatially resolved reconstruction of the star formation history (SFH) of the SMC, based on the application of their STARFISH analysis software to the multiband photometry of its 6 million stars from the Magellanic Clouds Photometric Survey, other works have argued that HZ04 did not go deep enough to derive the full SFH from the main sequence (MS) (Noël et al. 2009, hereafter NAGHCM). According to NAGHCM, HZ04 reached $B \sim 22$ mag, corresponding to stars younger than 3 Gyr old on the MS. However, while HZ04 covered the entire central 4×4.5 deg^2 area of the SMC main body, the works that reached the oldest MS turn-offs (MSTOs) have covered small fields of view: Dolphin et al. (2001, five *HST*-WFPC2 fields); McCumber, Garnett & Dufour (2005, one *HST*-WFPC2 field); Chiosi & Vallenari (2007, three *HST*-ACS fields); Sabbi et al. (2009, six *HST*-ACS fields); Cignoni et al. (2009, one *HST*-ACS field); and NAGHCM (12 8.85×8.85 deg^2 fields).

As far as we can see, the advantages of covering an enormous extension of the SMC are counterbalanced by the loss in depth of the limiting magnitude. For this reason, it is desirable to obtain an overall deeper SFH for the SMC. On the other hand, a comprehensive comparison between the star field and cluster AMRs is pending, obtained using the same procedure. All these aims demand the availability of a huge volume of high-quality data as well as a powerful technique to provide accurate ages and metallicities.

In this paper, we address these three issues for the first time. We present an unprecedented data base of some 3.3 million stars – measured with the Washington CT_1 photometric system – which are spread over the SMC main body. From this data base, we could produce the star field SMC AMR from the birth of the galaxy until ∼1 Gyr ago, using the δT_1 index and the standard giant branch (SGB) isoabundance lines to estimate ages and metallicities of the most representative field populations, respectively. This is the first derived field SMC AMR that only relies on empirical calibrations. In addition, as far as we are aware of, this is the first overall star field SMC AMR obtained from Washington data, thus complementing those derived from other photometric systems. Finally, we homogeneously compared the derived star field AMR to that recently obtained by Piatti (2011a) for the SMC cluster population with ages and metallicities derived using the same techniques. This comparison has not been accomplished before.

This paper is organized as follows. Section 2 describes the data handling from which we estimated star field ages and metallicities in Section 3. Section 4 deals with the aforementioned issue about a comprehensive star field SMC AMR, whereas Section 5 summarizes our results.

2 DATA HANDLING AND SCOPE

In our previous series of studies of SMC clusters, we have used the CT_1 Washington photometric system (Canterna 1976; Geisler 1996)

★E-mail: andres@iafe.uba.ar

© 2012 The Author
Monthly Notices of the Royal Astronomical Society © 2012 RAS

Table 1. SMC star fields.

Field	α_{2000} (^{h} ^{m} ^{s})	δ_{2000} ($^{\circ}$ $'$ $''$)	Number of measured stars	$E(B-V)$ (mag)
1	23 49 00.27	−72 56 43.3	12 027	0.02
2	00 42 01.38	−74 49 55.1	195 031	0.02
3	00 44 31.09	−71 52 00.2	193 988	0.06
4	00 47 53.70	−73 13 20.0	648 338	0.03
5	00 57 49.90	−74 19 28.2	373 398	0.02
6	01 00 02.05	−72 13 06.1	264 889	0.06
7	01 00 26.47	−71 17 43.0	245 020	0.05
8	01 01 42.20	−73 12 37.6	639 086	0.05
9	01 11 13.77	−73 07 13.1	456 790	0.03
10	01 13 01.88	−70 57 46.7	90 487	0.02
11	01 15 59.91	−74 20 00.1	129 941	0.03

whose ability to estimate ages and metallicities of star clusters has long been proved (Piatti et al. 2011, and references therein). For those reasons, and in order to keep consistence with our previous studies, we performed a search within the National Optical Astronomy Observatory (NOAO) Science Data Management Archives[1] looking for Washington photometric data towards the SMC. As a result, we found images obtained at the Cerro Tololo Inter-American Observatory 4-m Blanco telescope with the Mosaic II camera attached (36×36 arcmin^2 field on to a 8K × 8K CCD detector array) of 11 SMC star fields (see Table 1). Fig. 1 shows with the labelled boxes the spatial distribution of the 11 fields. It also includes the fields studied by Dolphin et al. (2001, filled boxes), McCumber et al. (2005, filled triangle), Chiosi & Vallenari (2007, open circles), Sabbi et al. (2009, filled circles), Cignoni et al. (2009, star), NAGHCM (open boxes) and HZ04 (big rectangle). Only the field areas covered by HZ04 and NAGHCM are proportional to the figure scale, whereas the remaining symbols are bigger than the areas covered by their respective fields.

We followed the route outlined by Piatti (2011b) for the reduction and analysis of the data. The stellar photometry was performed using the star-finding and point spread function (PSF) fitting routines in the DAOPHOT/ALLSTAR suite of programs (Stetson, Davis & Crabtree 1990). For each frame, a quadratically varying PSF was derived by fitting ∼960 stars, once the neighbours were eliminated using a preliminary PSF derived from the brightest, least contaminated ∼240 stars. Both groups of PSF stars were interactively selected. We then used the ALLSTAR program to apply the resulting PSF to the identified stellar objects and to create a subtracted image which was used to find and measure magnitudes of additional fainter stars. This procedure was repeated three times for each frame. Finally, we combined all the independent measurements using the standalone DAOMATCH and DAOMASTER programs, kindly provided by Peter Stetson. Table 1 lists the total number of stars with measured C and T_1 magnitudes. The left-hand panels of Figs 2(a)–(f) depict the resultant colour–magnitude diagrams (CMDs), while the right-hand panels show the respective Hess diagrams. These diagrams were produced by counting the number of stars placed in different colour–magnitude bins with sizes $[\Delta T_1, \Delta(C-T_1)] = (0.1,0.05)$ mag and then by representing the count scale with a 10 grey level logarithmic scale. Field #1 served as a reference to subtract the galactic signature from the remaining 10 fields. For the subsequent analysis, we subdivided each 36×36 arcmin^2 field into 16 uniform 2K × 2K regions (9×9 arcmin^2 each) in order to deal with comparable-sized individual areas to HZ04 and NAGHCM. We labelled such subfields with letters A to P moving from the west to the east and from the south to the north.

We quantify the completeness down to the faintest magnitudes, since our photometry only just extends beyond the magnitude of the oldest MSTOs. Photometric errors, crowding effects and the detection limit of the images cause incompleteness and therefore result in the loss of stars at faint magnitudes. Commonly, artificial star tests on the deepest images are performed in order to derive the completeness level at different magnitudes. We use the stand-alone ADDSTAR program in the DAOPHOT package (Stetson et al. 1990) to add synthetic stars, placed at random with positions and magnitudes, to a subsample of images in order to derive the completeness levels for crowded, intermediate-crowded and uncrowded fields. The selected fields were chosen using as a reference the number of measured stars shown in column 4 of Table 1. In each image, we add a number of stars equivalent to ∼5 per cent of the measured stars to avoid in the synthetic images significantly more crowding than in the original images, making it difficult to apply the artificial-star conclusions to our program-star results. On the other hand, to avoid small number statistics in the artificial-star analysis, we create five different images for each original one. We then repeat the same steps to obtain the photometry of the synthetic images and the star-finding efficiency was estimated by comparing the output and input data for these stars. The completeness level for the C and T_1 filters is plotted for the selected fields in Fig. 3 as a function of magnitude. The completeness profiles for the remaining fields are between those shown in Fig. 3 for both filters. Fig. 3 shows that the 50 per cent completeness level is located at $C \sim 23$–24.5 and $T_1 \sim 22.5$–24.0, depending on the crowding.

3 AGES AND METALLICITIES OF THE SMC STAR FIELDS

We are primarily interested in determining the age and metallicity of the representative star population in each field. Here the term 'representative' refers to the most numerous stellar population along the line of sight as defined by Geisler et al. (2003), and subsequently used by Piatti et al. (2003a, 2003b, 2007), among others. Thus, we build the presently observed AMR from ages and metallicities of the prevailing stellar populations, independently of whether they are primordial or recently formed. These prevailing populations trace the present-day AMR of the galaxy. They account for the most important metallicity-enrichment processes that have undergone in the galaxy lifetime. Minority stellar populations not following these main chemical galactic processes are discarded. Therefore, presently-subdominant populations in certain locations could have been in the majority in the galaxy in the past, but were not considered. This could also be the case with old stellar populations placed in the innermost regions. However, unless the SMC has had an original metallicity gradient during its birth, the metallicity of the oldest stellar populations is recovered from the dominant oldest populations. Such dominant oldest populations (age ∼ 13 Gyr) should have observed TOs at $T_1 \approx 22.3$ mag and $C \approx 22.9$ mag – according to the theoretical isochrones of Girardi et al. (2002) – if a reddening of $E(B-V) = 0.03$ mag, a SMC distance modulus of 18.9 mag, and a metallicity of [Fe/H] = −1.5 are assumed. Furthermore, if the oldest TO of a field is also the TO of the dominant population of that field, then they should be detected using the present data within 100 per cent completeness. On the other hand, note that an AMR is not directly comparable to SFH (Harris & Zaritsky 2009). Our AMR differs from AMRs derived from modelled SFHs in that it

[1] http://www.noao.edu/sdm/archives.php.

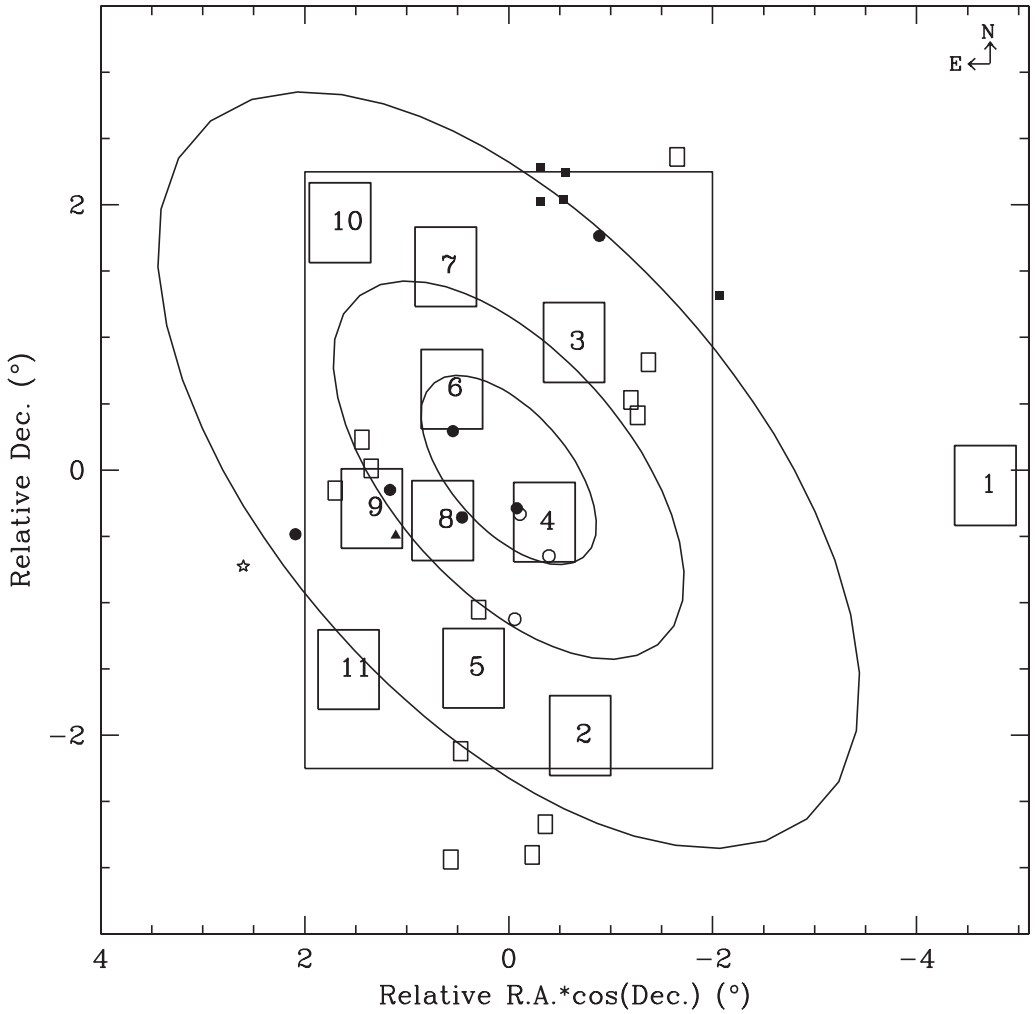

Figure 1. Spatial distribution of the presently studied SMC star fields (thick numbered boxes), and those of Dolphin et al. (2001, filled boxes), McCumber et al. (2005, filled triangle), Chiosi & Vallenari (2007, open circles), Sabbi et al. (2009, filled circles), Cignoni et al. (2009, star), NAGHCM (open boxes) and the HZ4 area (big rectangle). Ellipses with semi-major axes of 1°, 2° and 4° are overplotted.

does not include the complete information on the stellar population evolution.

We derived ages from the δT_1 index, calculated by determining the difference in the T_1 magnitudes of the red clump (RC) and the MSTO (Geisler et al. 1997). Note that this age-measurement technique does not require absolute photometry. An additional advantage is that we do not need go deep enough to see the extended MS of the representative star population but only its MSTO. Since field CMDs are obviously composed of MS stars of different stellar populations, we derived δT_1 values for the MS with the TO containing the largest concentration of stars. We assumed that the observed MS is a result of superimposition of MSs with different TOs (ages) and constant luminosity functions. Hence, the difference between the number of stars of two adjacent magnitude intervals gives the intrinsic number of stars belonging to the faintest interval. Consequently, the biggest difference is directly related to the most populated TO. The method would not converge to any dominant TO (age) value if the considered field is derived considering a constant star formation rate (SFR) over all time. In such a case, the difference between the number of stars of two adjacent magnitude intervals would result in the same value for any T_1 bin. For our studied fields, we could clearly identify the respective most populated TOs; no sign of constant SFR was detected within three adjacent bins when their T_1 magnitude errors are taken into account. In addition, the resultant T_1(MSTO) is at least ∼0.5 mag brighter than the T_1 magnitude for the 100 per cent completeness level of the respective field.

To find this maximum value, we counted the number of stars in bins of 0.25 mag along the star field MSs. The chosen bin size encompasses the T_1 magnitude errors of the stars in each bin, thus producing an appropriate sample of the stars. It would be difficult for a star included in an age bin to fall in the closest adjacent bin due to its photometric errors. The chosen MS lower and upper envelopes also encompass objects corresponding to MS stars with metallicities more metal poor than [Fe/H] ~ -0.3 dex, with $E(B-V) \lesssim 0.20$ mag, located at the SMC distance modulus, including photometric errors (Girardi et al. 2002; Glatt, Grebel & Koch 2010; Piatti 2011b). To illustrate the results, Fig. 4 depicts for each studied field (labelled at the top left-hand corner of each panel) the normalized star field luminosity function within the 100 per cent completeness level (top panel) and the differential luminosity function used to define the most populated TOs (bottom panel) corresponding to the respective so-called J subfield. The prevailing TOs are typically ∼25–50 per cent more frequent – within the quoted errors – than the following less dominant population. We assigned

© 2012 The Author, MNRAS **422,** 1109–1121
Monthly Notices of the Royal Astronomical Society © 2012 RAS

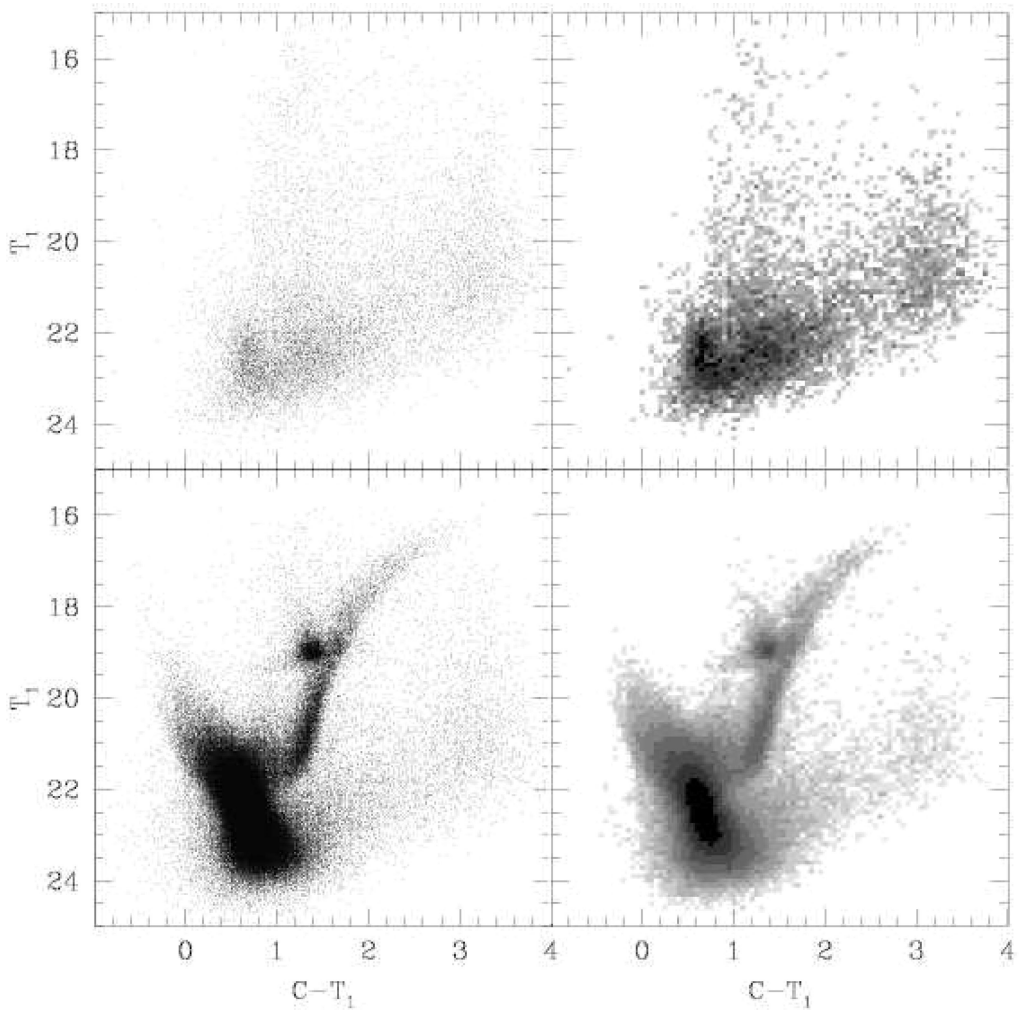

Figure 2. (a) CMDs for the studied SMC star fields #1 (top left-hand panel) and #2 (bottom left-hand panel), and the respective Hess diagrams (right-hand panels); (b) CMDs for the studied SMC star fields #3 (top left-hand panel) and #4 (bottom left-hand panel), and the respective Hess diagrams (right-hand panels); (c) CMDs for the studied SMC star fields #5 (top left-hand panel) and #6 (bottom left-hand panel), and the respective Hess diagrams (right-hand panels); (d) CMDs for the studied SMC star fields #7 (top left-hand panel) and #8 (bottom left-hand panel), and the respective Hess diagrams (right-hand panels); (e) CMDs for the studied SMC star fields #9 (top left-hand panel) and #10 (bottom left-hand panel), and the respective Hess diagrams (right-hand panels); and (f) CMD for the studied SMC star field #11 (left-hand panel) and the respective Hess diagram (right-hand panel).

to the MSTO T_1 magnitudes dispersions four times those typical of the photometry at the TO level, that is, $\langle\sigma(T_1)\rangle \approx 0.05$ mag. As for the RC T_1 magnitudes, we built T_1 histograms for the RC stars, then we performed Gaussian fits and derived their mean values and full widths at half-maximum (FWHMs). The FWHMs are in general of the order of 10 times that typical of the photometry at the RC level, that is, $\langle\sigma(T_1)\rangle \approx 0.02$ mag. Although RC stars are usually used as standard candles for distance determination (Paczynski & Stanek 1998; Olsen & Salyk 2002; Subramaniam 2003), we assume that the T_1(RC) magnitude corresponds to the most populous T_1(MSTO) in the respective field. Tables 2 and 3 list the resulting MSTO and RC T_1 magnitudes, respectively. The MSTO T_1 magnitudes are brighter than those for the 100 per cent completeness level, as shown in Fig. 4, so that we actually reach the TO of the representative population of each field. We then derived ages from the δT_1 values using equation (4) of Geisler et al. (1997). Such equation is calibrated for ages bigger than 1 Gyr, so that we are not able to produce the field AMR for younger ages. Using the theoretical isochrones of Girardi et al. (2002) for $Z = 0.004$, the 0.25 mag intervals used above can be converted into age bins (Δ(age) Gyr, $\langle T_1$(MSTO)$\rangle$ mag): (0.04, 18), (0.11, 19), (0.29, 20), (0.29, 21), (0.85, 22), (2.60, 23), etc.

Finally, mean metallicities for the star fields were also obtained using the $[M_{T_1}, (C - T_1)_o]$ plane with the SGBs of Geisler & Sarajedini (1999). They demonstrated that the metallicity sensitivity of the SGBs (each giant branch corresponds to an isoabundance curve) is three times higher than that of the V, I technique (Da Costa & Armandroff 1990) and that, consequently, it is possible to determine metallicities three times more precisely for a given photometric error. However, the SGBs were defined mainly by using globular clusters older than 10 Gyr. In view of the well-known age–metallicity degeneracy, it is important to examine as closely as possible the effect of applying such a calibration based on very old objects to much younger clusters. Geisler et al. (2003) explored this effect empirically by comparing the differences in $(C - T_1)_o$ to theoretical isochrones (see their fig. 6).

We then followed the standard SGB procedure of entering absolute M_{T_1} magnitudes and intrinsic $(C - T_1)_o$ colours for each field into fig. 4 of Geisler & Sarajedini (1999). The absolute M_{T_1} magnitudes and intrinsic $(C - T_1)_o$ colours were obtained from the

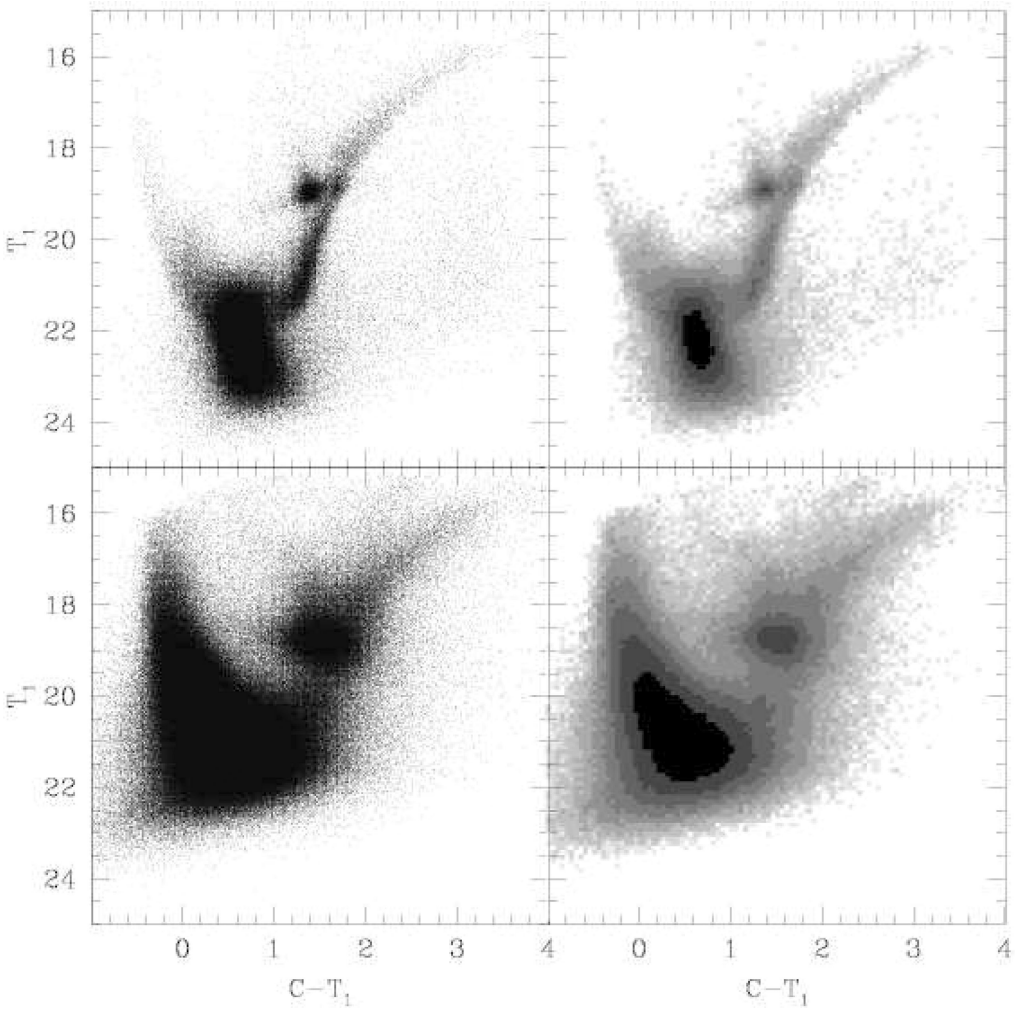

Figure 2 – *(b) continued*

equations $M_{T_1} = T_1 + 0.58E(B-V) - (V-M_V)$ and $(C-T_1)_o = C - T_1 - 1.97E(B-V)$ (Geisler & Sarajedini 1999), where $E(B-V)$ and $(V-M_V)$ represent the colour excess and the apparent distance modulus, respectively. Field reddening values were estimated by interpolating the extinction maps of Burstein & Heiles (1982). These maps were obtained from H I (21-cm) emission data for the southern sky and provide us with foreground $E(B-V)$ colour excesses which depend on the Galactic coordinates (see the last column of Table 1). As for the SMC distance modulus, we adopted the value $(m-M)_o = 18.90 \pm 0.10$ (Glatt et al. 2010). We refer the reader to Crowl et al. (2001) and Piatti et al. (2007), for example, for a detailed analysis about using a unique distance modulus. Then, we entered these $(C-T_1)_o$ and M_{T_1} values in fig. 4 of Geisler & Sarajedini as illustrated in Fig. 5, which shows the reddening-corrected Hess diagram for the SMC field #5. We interpolate the field metal abundance values ([Fe/H]), using the mean position estimated by eye of the whole extension of the RGB, into the isoabundance lines drawn in the figure. The metallicities herein derived were then corrected for age effects following the prescriptions given in Geisler et al. (2003). This was done by entering the derived ages into fig. 4 of Geisler et al. to obtain a Δ[Fe/H] value (the metallicity correction), which we subtracted from the measured [Fe/H]. In order to take into account the metallicity spread, we assume a dispersion of 0.4 dex (absolute value) for the measured metallicities, although the SGB procedure allows us to estimate [Fe/H] values with an uncertainty of 0.1 dex, to which we added the uncertainties coming from the age corrections in order to assign formal errors to the final metallicity values.

Table 4 lists the mean age and metallicity for each studied field. Note that the field RGBs (see Fig. 2) are very well populated and show a significant colour (age) spread at a given magnitude, although it is difficult to tell how much of the observed spread is due to age spread and how much due to metallicity spread. Here we have simply given the mean metal abundance derived from the above analysis. Similarly, the adopted age errors represent in general a satisfactory estimate of the age spread around the prevailing population ages, although some few individual subfields have slightly larger age spread. As far as we are aware of, these larger age spreads do not affect the subsequent results. In order to help validate the present results, we compared the resultant mean ages and metallicities with those from Sabbi et al. (2009). Our fields #8-E/I and #9-I/M nearly match their fields SFH5 and SFH10, respectively. Sabbi et al. found that most of the stars in SHF5 are older than $\sim$2 Gyr and that $\sim$22 per cent of the stars have ages between 8 and 12 Gyr. For SFH10, they found that the stars formed at a steady pace between $\sim$5 and $\sim$3 Gyr ago, and that $\sim$20 per cent of the stars are older than 8 Gyr. For both fields they used isochrones of $Z = 0.001$ and 0.004 to fit older and younger stellar populations, respectively. According to

© 2012 The Author, MNRAS **422,** 1109–1121
Monthly Notices of the Royal Astronomical Society © 2012 RAS

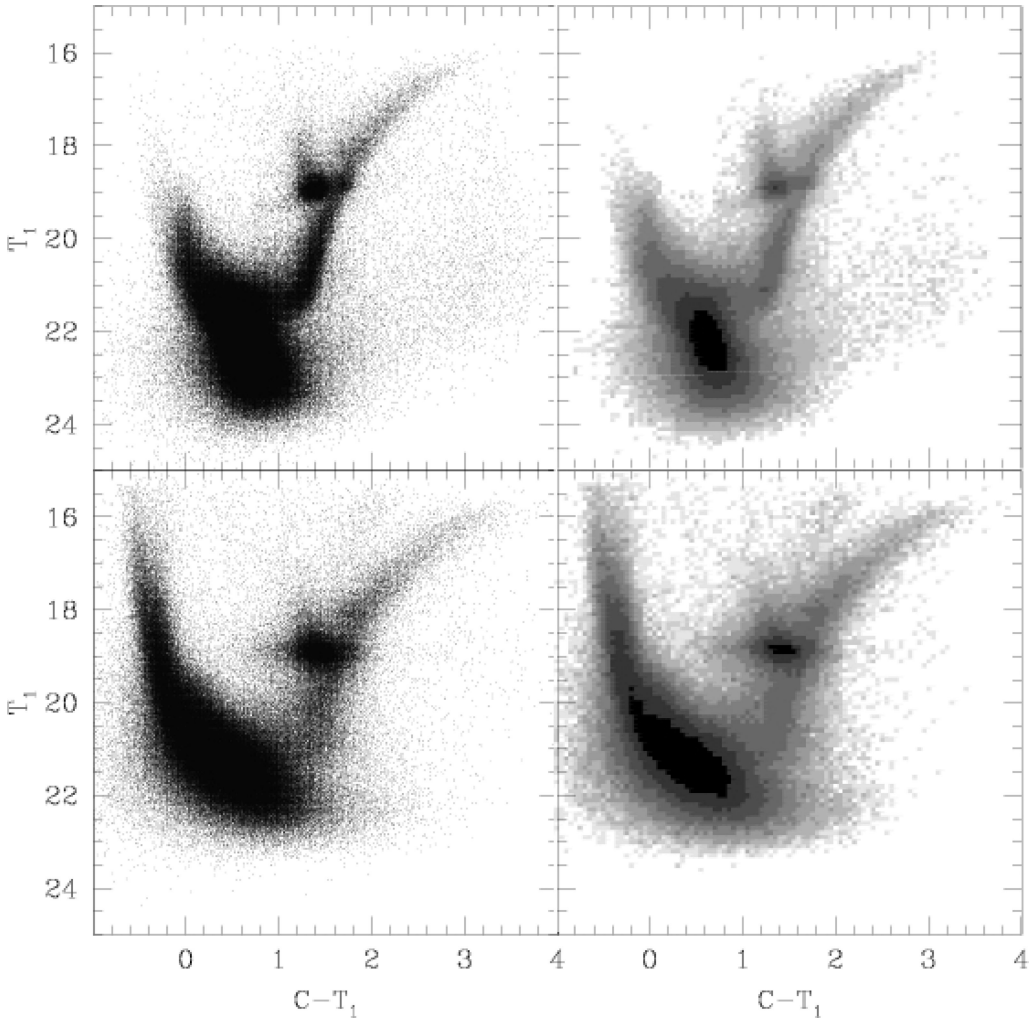

Figure 2 – *(c) continued*

Table 4, the prevailing stellar populations of field #8-E/I have mean ages of ∼2.5 Gyr, while a range between ∼4.7 and ∼7.3 Gyr is found for field #9-I/M. As for their mean metal contents, we found $[Fe/H]_{8\text{-E/I}} \sim -0.9$ dex and $[Fe/H]_{9\text{-I/M}} \sim -1.2$ dex. As can be seen, there exists a reasonable degree of agreement between both results.

4 COMPREHENSIVE PICTURE OF THE STAR FIELD AMR

In Fig. 6, we show the resultant AMR for the studied 160 9×9 arcmin^2 SMC regions. We recall that the presently observed field AMR is independent of any previous approach. In addition, this is the first overall star field SMC AMR obtained from Washington data, thus complementing those derived from other photometric systems. In the left-hand panel, we overplotted with different lines star field AMRs obtained previously, namely HZ04 (solid line), Dolphin et al. (2001, long-dashed line), Carrera et al. (2008, short-dashed line) and NAGHCM (dotted line), while in the right-hand panel we have superimposed the AMRs modelled by Pagel & Tautvaišienė (1998, hereafter PT98) (solid line) and Tsujimoto & Bekki (2010, dotted, short-dashed and long-dashed lines). Their three curves correspond to mergers with the mass ratio of 1–4 (long-dashed curve), to an equal-mass merger (short-dashed curve) and to a no-merger event (dotted curve). We remind the reader that the superimposed modelled AMRs come from global SMC SFHs, while our AMR reflects the present-day AMR as traced by its prevailing stellar populations. At first glance, it seems that the bursting SFH modelled by PT98 is qualitatively the closest to our AMR. However, such resemblance is apparent since PT98 constructed their model using no star formation from ∼11 up to 4 Gyr ago (see their fig. 2). This clearly conflicts with the present results that show there was in fact probably a lot of star formation in the SMC in this period, particularly between 6 and 8 Gyr ago (see below).

Furthermore, when the elliptical framework proposed by Piatti et al. (2005) is used (Piatti et al. 2007, 2008; Parisi et al. 2009; Piatti 2011a,b, and references therein), we find that prevailing field star populations do not possess gradients in age and metallicity, and that stellar populations formed since ∼2 Gyr ago are more metal rich than [Fe/H] ~ -0.8 dex and are confined to the innermost region (semi-major axis $\lesssim 1^\circ$). Fig. 7 shows that the bigger the value of the corresponding semi-major axis, the older and the more metal poor the star field, with a non-negligible dispersion. In the left-hand panel of the figure, we represent with the black filled squares the prevailing star fields more metal rich than [Fe/H] $= -1.0$ dex, while in the right-hand panel the black, dark-grey and clear-grey boxes correspond to prevailing star fields younger than 3 Gyr, with ages between 3 and 8 Gyr, and older than 8 Gyr, respectively. Note that

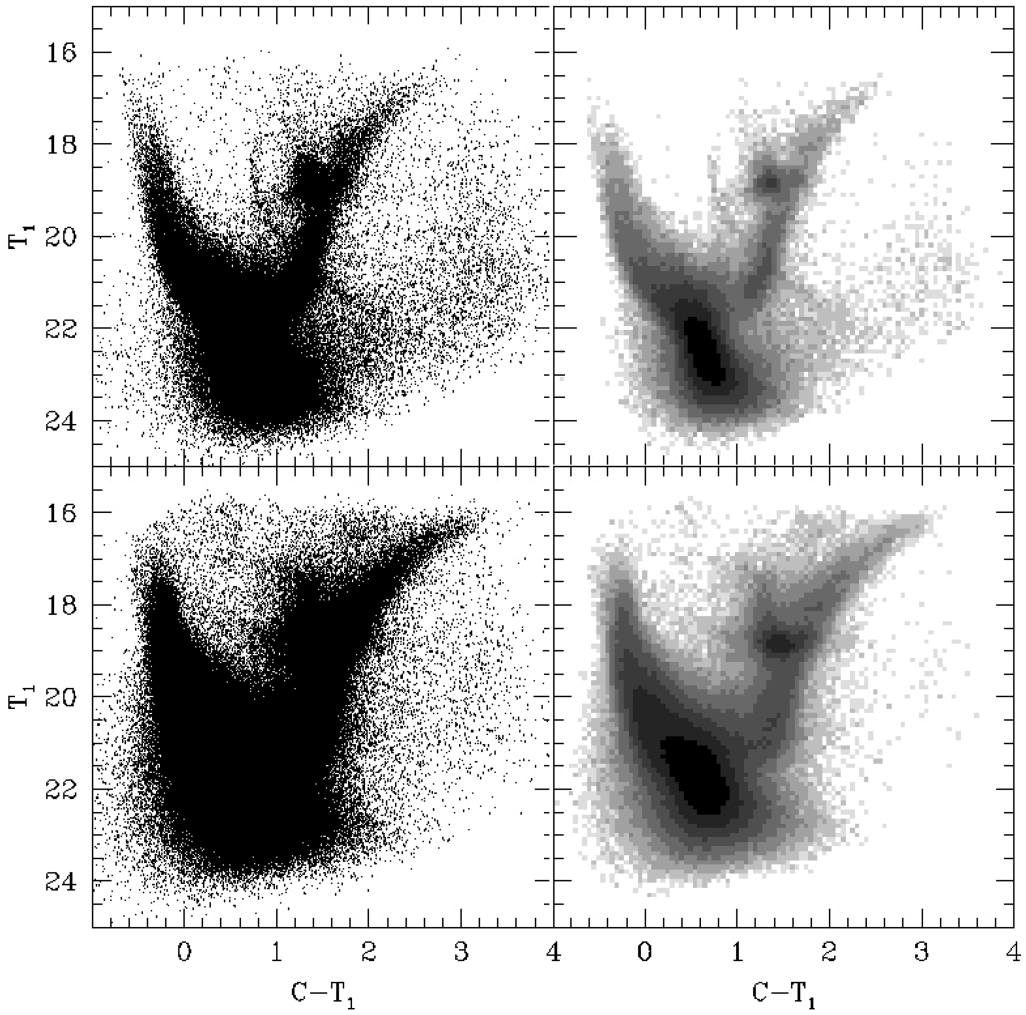

Figure 2 – *(d) continued*

relatively metal poor populations ([Fe/H] = (−1.00 ± 0.15) dex) are found in the central regions [semi-major axis = (1°.0 ± 1°.0)], having been formed relatively recently [$t = (3.0 \pm 1.0)$ Gyr]. We recall that these observed gradients could not represent the original age and metallicity distributions in these innermost regions, since presently-subdominant old populations could have been in the majority in the past in the whole galaxy.

As Piatti (2011a) showed, these resultant trends are confirmed by the observed spatial distribution of the SMC cluster population. The cluster ages and metallicities used by Piatti were derived using the same techniques as described here so that they are all in the same homogeneous age/metallicity scales. Clusters and star fields also show other some coincidences. Both galaxy components have experienced two enhanced formation processes: the most recent peaked at an age of ∼2 Gyr, and an earlier one detected at an age of ∼5–6 and 7.5 Gyr for clusters and star fields, respectively. For a detailed study of the enhanced cluster formation, we refer the reader to Piatti (2011a). As for the enhanced star field formation, the left-hand panel of Fig. 8 depicts the histogram of the number of 9×9 arcmin^2 subfields found per age interval over the 160 studied subfields, revealing both peaks within a narrow age range centred at the aforementioned ages. Note that the higher peaked distribution at ∼7.5 Gyr does not imply that the related enhanced star formation process has been more important in terms of mass than that at ∼2 Gyr. The right-hand panel shows that the spread in metallicity (Δ[Fe/H] = [Fe/H]$_{\rm max}$ − [Fe/H]$_{\rm min}$) additionally accounts for these violent episodes. These possibly depict that vigorous nucleosynthesis processes took place and that the metallicity mixing became less efficient. None of the previously derived AMRs has accounted for the earlier burst, except in the case of the theoretical model of Tsujimoto & Bekki (2010). With respect to the most recent burst, it does not appear to arise from the Dolphin et al. (2001), Carrera et al. (2008) and NAGHCM mean AMRs, although the mean metallicities of short bursts in Dolphin et al.'s AMR would be averaged out. Apparently, only HZ04's AMR does seem to account for the amplitude in [Fe/H] values of the ∼2 Gyr bursting formation episode.

5 SUMMARY

In this study, we present, for the first time, CCD Washington CT_1 photometry of some 3.3 million stars in 11 36×36 arcmin^2 fields distributed throughout the entire SMC main body. The analysis of the photometric data – subdivided into 160 smaller 9×9 arcmin^2 fields – leads to the following main conclusions:

(i) We estimated ages of the representative star population in each field using the δT_1 index and metallicities from the SGB

© 2012 The Author, MNRAS **422,** 1109–1121
Monthly Notices of the Royal Astronomical Society © 2012 RAS

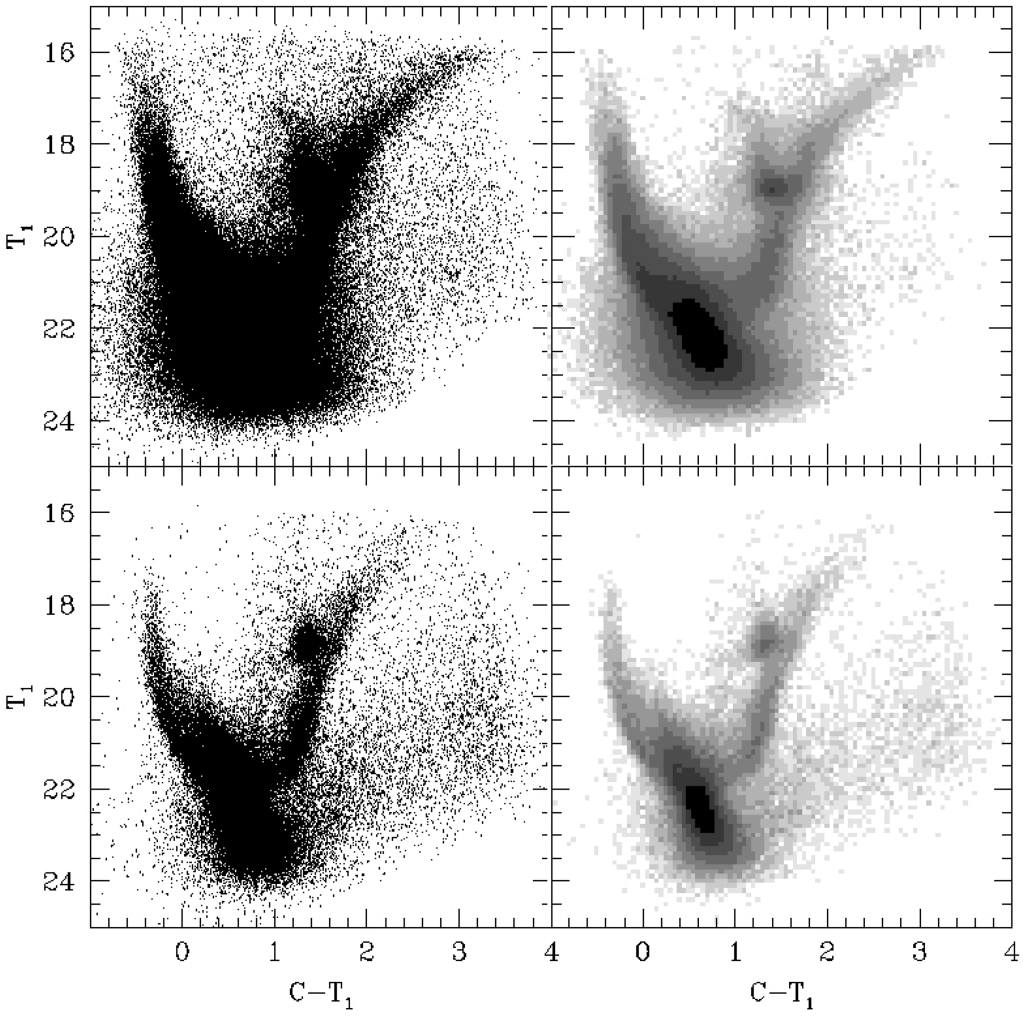

Figure 2 – *(e) continued*

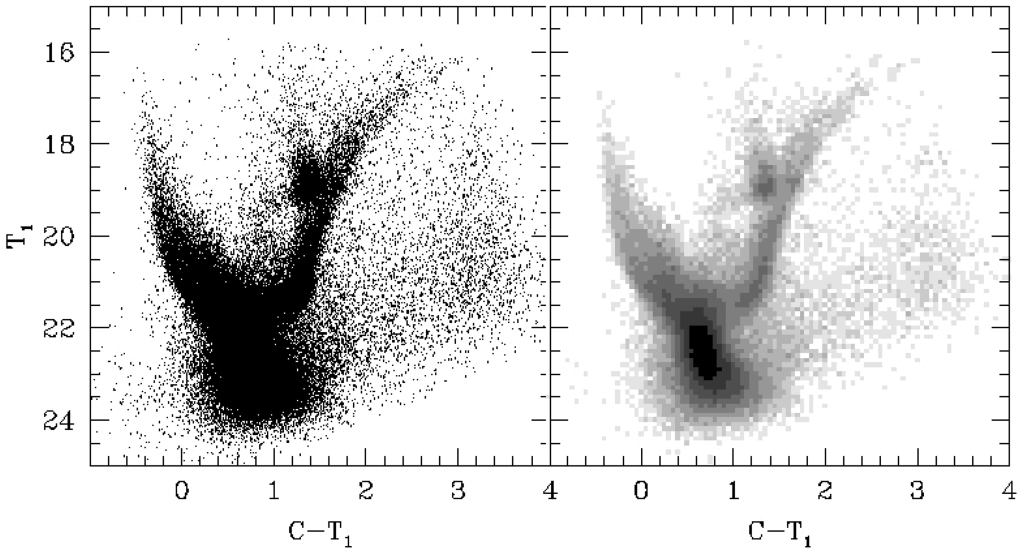

Figure 2 – *(f) continued*

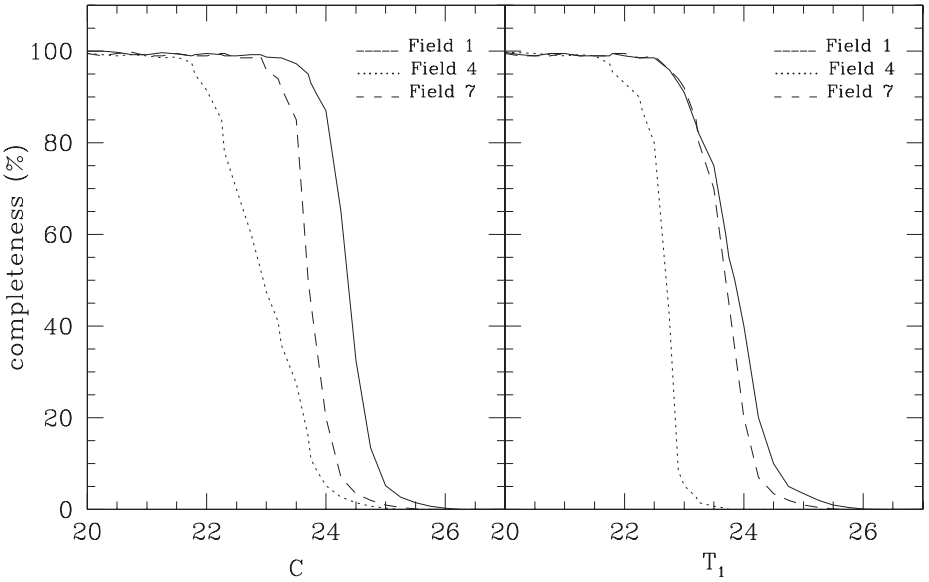

Figure 3. Completeness levels of three fields as a function of magnitude for the C and T_1 filters.

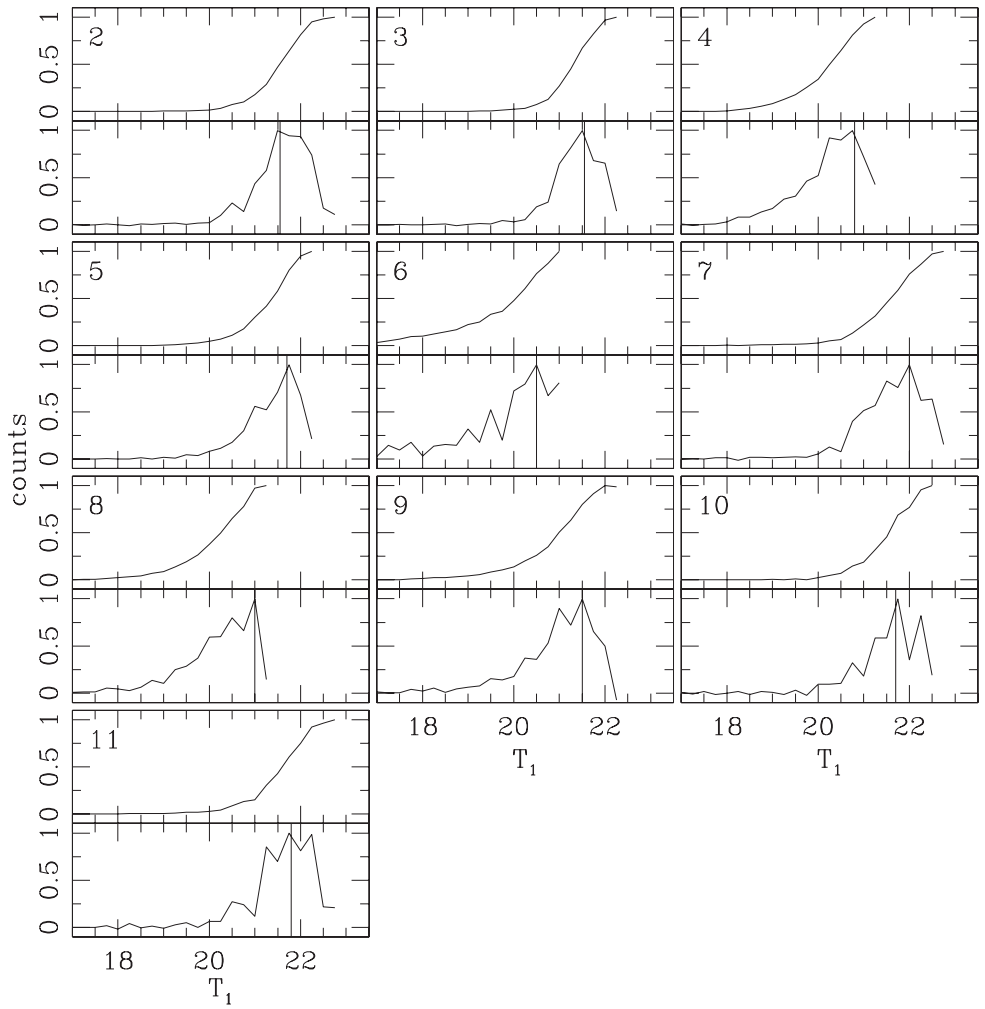

Figure 4. The normalized luminosity functions of the MS stars corresponding to the J subfield of the studied SMC fields, labelled at the respective top left-hand corners. The respective differential luminosity functions used to define the most populated TOs are depicted below each of them, where the adopted T_1(MSTO) magnitude is indicated with a vertical line (see also Table 2).

© 2012 The Author, MNRAS **422,** 1109–1121
Monthly Notices of the Royal Astronomical Society © 2012 RAS

Table 2. MSTO T_1 magnitudes for the studied SMC star fields.

Field	A	B	C	D	E	F	G	H	I	J	K	L	M	N	O	P
1	–	–	–	–	–	–	–	–	–	–	–	–	–	–	–	–
2	22.125	22.125	22.125	22.125	22.125	21.875	22.125	21.875	21.875	21.625	21.875	21.875	22.125	21.875	21.875	21.875
3	21.375	21.625	21.875	21.625	21.875	21.875	21.627	21.375	21.875	21.875	21.875	21.875	21.875	21.625	21.625	21.875
4	20.375	20.375	20.625	20.625	20.375	19.875	20.375	20.375	20.125	20.125	19.875	19.375	20.875	20.625	20.125	19.875
5	21.875	21.875	21.875	21.875	21.875	21.875	22.125	21.875	21.875	21.875	21.625	21.875	21.375	21.875	21.875	21.875
6	20.375	20.375	20.875	21.125	20.625	20.125	20.625	21.125	21.125	20.625	21.125	21.125	21.125	21.125	21.125	21.125
7	21.875	21.625	21.325	22.125	21.625	22.125	21.875	22.375	21.875	22.125	22.125	21.875	21.875	22.125	22.125	21.875
8	20.875	21.125	21.125	21.125	20.625	20.625	21.375	21.375	20.875	21.125	20.875	21.125	20.625	20.875	20.875	21.125
9	21.125	21.875	22.125	21.875	21.875	21.625	21.875	22.125	21.875	21.625	21.875	21.875	21.375	21.375	21.125	21.375
10	21.625	21.625	21.875	22.125	22.375	21.875	21.375	21.875	21.875	21.875	21.625	21.375	21.125	22.125	21.875	21.875
11	21.875	22.375	22.125	22.125	21.875	22.125	21.875	21.875	22.375	21.875	22.375	21.875	21.875	21.875	22.125	21.875

Table 3. RC T_1 magnitudes for the studied SMC star fields.

Field	A	B	C	D	E	F	G	H	I	J	K	L	M	N	O	P
1	–	–	–	–	–	–	–	–	–	–	–	–	–	–	–	–
2	19.00	18.95	19.00	19.00	19.00	19.00	19.00	18.95	19.00	19.00	19.00	18.95	18.95	18.95	19.00	18.95
3	19.00	18.95	18.95	18.90	18.95	18.95	18.95	18.95	19.00	18.95	18.95	18.95	18.95	18.95	18.95	18.95
4	18.70	18.80	18.75	18.85	18.70	18.75	18.75	18.85	18.70	18.80	18.80	18.85	18.70	18.80	18.80	18.80
5	18.95	18.95	18.95	18.95	18.95	18.95	18.95	18.95	18.95	18.95	18.95	18.95	18.95	18.95	18.95	18.95
6	18.95	18.95	18.95	18.95	18.05	18.90	18.90	18.90	18.95	18.90	18.90	18.95	18.90	18.90	18.90	18.85
7	18.95	18.90	18.90	18.90	18.95	18.90	18.90	18.90	18.90	18.90	18.90	18.90	18.90	18.90	18.85	18.85
8	18.90	18.95	18.90	19.00	18.90	18.95	18.90	19.00	18.90	18.95	18.90	19.00	18.95	18.90	18.90	18.90
9	19.05	19.05	19.05	19.05	19.00	19.05	19.05	19.00	19.00	19.00	19.00	19.00	18.90	18.95	18.95	18.95
10	18.85	18.90	18.90	18.90	18.90	18.90	18.90	18.90	18.90	18.90	18.90	18.90	19.00	18.90	18.90	18.90
11	19.05	19.05	19.05	19.05	18.95	19.05	19.05	19.05	18.95	19.00	19.05	19.05	18.95	19.00	19.00	19.00

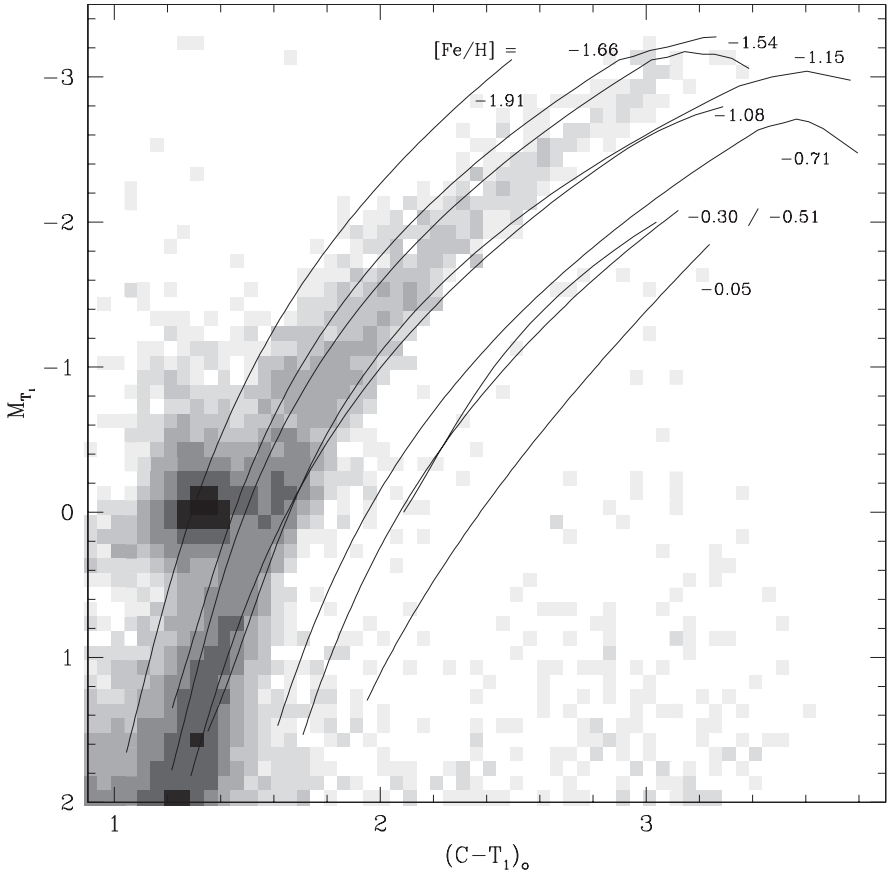

Figure 5. Reddening-corrected Hess diagram for the SMC star field #5, with SGBs from Geisler & Sarajedini (1999) superimposed.

Table 4. Mean ages (Gyr) and metallicities (dex) and their respective dispersions for the representative populations in the studied SMC star fields.

Field	2	3	4	5	6	7	8	9	10	11
A	9.55 ± 2.99	4.20 ± 1.40	2.08 ± 0.51	7.73 ± 2.50	1.73 ± 0.33	7.73 ± 2.50	2.74 ± 0.82	3.04 ± 0.95	6.56 ± 2.17	6.93 ± 2.27
	-1.23 ± 0.41	-1.24 ± 0.33	-0.59 ± 0.31	-1.13 ± 0.28	-0.86 ± 0.28	-1.28 ± 0.29	-0.91 ± 0.34	-1.01 ± 0.34	-1.21 ± 0.27	-1.26 ± 0.27
B	10.06 ± 3.12	5.87 ± 1.96	1.92 ± 0.43	7.73 ± 2.50	1.73 ± 0.33	6.21 ± 2.06	3.38 ± 1.09	6.93 ± 2.27	6.21 ± 2.06	11.72 ± 3.52
	-1.31 ± 0.47	-0.71 ± 0.28	-0.75 ± 0.29	-1.23 ± 0.28	-0.71 ± 0.28	-1.30 ± 0.28	-1.00 ± 0.34	-1.26 ± 0.27	-1.20 ± 0.28	-1.43 ± 0.20
C	9.55 ± 2.99	2.61 ± 0.76	2.48 ± 0.71	7.73 ± 2.50	2.61 ± 0.76	4.44 ± 1.49	3.56 ± 1.16	9.07 ± 2.86	8.15 ± 2.62	9.07 ± 2.86
	-1.23 ± 0.41	-0.94 ± 0.33	-0.87 ± 0.33	-1.23 ± 0.28	-0.94 ± 0.33	-1.21 ± 0.32	-1.03 ± 0.34	-1.21 ± 0.26	-1.24 ± 0.30	-1.16 ± 0.26
D	9.55 ± 2.99	3.38 ± 1.09	2.27 ± 0.60	7.73 ± 2.50	3.37 ± 1.09	10.59 ± 3.25	3.20 ± 1.02	6.93 ± 2.27	10.59 ± 3.25	9.07 ± 2.86
	-1.28 ± 0.31	-1.05 ± 0.34	-0.93 ± 0.32	-1.18 ± 0.28	-1.05 ± 0.34	-1.40 ± 0.26	-0.93 ± 0.34	-1.21 ± 0.27	-1.50 ± 0.26	-1.26 ± 0.26
E	9.55 ± 2.99	5.26 ± 1.76	2.08 ± 0.51	7.73 ± 2.50	5.26 ± 1.76	5.87 ± 1.96	2.17 ± 0.56	7.32 ± 2.39	13.59 ± 3.95	7.73 ± 2.50
	-1.33 ± 0.31	-1.31 ± 0.30	-0.74 ± 0.31	-1.23 ± 0.28	-1.31 ± 0.30	-1.29 ± 0.28	-0.91 ± 0.31	-1.27 ± 0.27	-1.92 ± 0.24	-1.23 ± 0.28
F	7.32 ± 2.39	7.73 ± 2.50	1.47 ± 0.21	7.73 ± 2.50	1.54 ± 0.24	10.59 ± 3.25	2.08 ± 0.51	5.26 ± 1.76	8.15 ± 2.62	9.07 ± 2.86
	-1.27 ± 0.27	-1.48 ± 0.28	-0.65 ± 0.25	-1.23 ± 0.28	-0.87 ± 0.26	-1.45 ± 0.26	-0.84 ± 0.31	-1.16 ± 0.30	-1.29 ± 0.30	-1.26 ± 0.36
G	9.55 ± 2.99	5.89 ± 1.96	2.00 ± 0.47	10.06 ± 3.12	2.17 ± 0.56	8.15 ± 2.62	4.70 ± 1.58	6.93 ± 2.27	4.70 ± 1.58	6.93 ± 2.27
	-1.28 ± 0.31	-1.39 ± 0.28	-0.77 ± 0.30	-1.31 ± 0.27	-1.01 ± 0.31	-1.34 ± 0.30	-1.18 ± 0.31	-1.21 ± 0.27	-1.18 ± 0.31	-1.21 ± 0.27
H	7.73 ± 2.50	4.44 ± 1.49	1.85 ± 0.40	7.73 ± 2.50	3.56 ± 1.16	13.59 ± 3.95	4.20 ± 1.40	9.55 ± 2.99	8.15 ± 2.62	6.93 ± 2.27
	-1.18 ± 0.28	-1.31 ± 0.32	-0.84 ± 0.29	-1.18 ± 0.28	-1.23 ± 0.34	-1.92 ± 0.22	-1.14 ± 0.33	-1.23 ± 0.31	-1.34 ± 0.30	-1.21 ± 0.27
I	7.32 ± 2.39	7.32 ± 2.39	1.73 ± 0.33	7.73 ± 2.50	3.38 ± 1.09	8.15 ± 2.62	2.74 ± 0.82	7.32 ± 2.39	8.15 ± 2.62	12.94 ± 3.80
	-1.27 ± 0.27	-1.32 ± 0.27	-0.66 ± 0.28	-1.23 ± 0.28	-1.05 ± 0.34	-1.34 ± 0.30	-0.96 ± 0.34	-1.27 ± 0.27	-1.34 ± 0.30	-1.75 ± 0.17
J	5.56 ± 1.86	7.73 ± 2.50	1.63 ± 0.28	7.73 ± 2.50	2.17 ± 0.56	10.59 ± 3.25	3.38 ± 1.09	5.56 ± 1.86	8.15 ± 2.62	7.32 ± 2.39
	-1.22 ± 0.29	-1.48 ± 0.28	-0.69 ± 0.27	-1.28 ± 0.28	-0.96 ± 0.31	-1.45 ± 0.26	-1.05 ± 0.34	-1.17 ± 0.29	-1.29 ± 0.30	-1.27 ± 0.27
K	7.32 ± 2.96	7.73 ± 2.50	1.43 ± 0.20	5.87 ± 1.96	3.56 ± 1.16	10.59 ± 3.25	2.74 ± 0.82	7.32 ± 2.39	6.21 ± 2.06	11.72 ± 3.52
	-1.27 ± 0.27	-1.43 ± 0.28	-0.64 ± 0.25	-1.19 ± 0.28	-1.08 ± 0.34	-1.45 ± 0.26	-0.91 ± 0.34	-1.17 ± 0.27	-1.25 ± 0.28	-1.53 ± 0.20
L	7.73 ± 2.50	7.73 ± 2.50	1.04 ± 0.29	7.73 ± 2.50	3.38 ± 1.09	8.15 ± 2.62	3.20 ± 1.02	7.32 ± 2.39	4.70 ± 1.58	6.93 ± 2.27
	-1.18 ± 0.28	-1.38 ± 0.28	-0.63 ± 0.28	-1.18 ± 0.28	-1.15 ± 0.34	-1.29 ± 0.30	-0.98 ± 0.34	-1.17 ± 0.27	-1.18 ± 0.31	-1.16 ± 0.27
M	10.06 ± 3.12	7.73 ± 2.50	3.38 ± 1.09	4.44 ± 1.49	3.56 ± 1.16	8.15 ± 2.62	2.08 ± 0.51	4.70 ± 1.58	3.20 ± 1.02	7.73 ± 2.50
	-1.26 ± 0.47	-1.38 ± 0.28	-0.95 ± 0.34	-1.06 ± 0.32	-1.03 ± 0.34	–	-0.79 ± 0.31	-1.13 ± 0.31	-1.08 ± 0.34	-1.28 ± 0.28
N	7.73 ± 2.50	5.87 ± 1.96	2.37 ± 0.65	7.73 ± 2.50	3.56 ± 1.16	10.59 ± 3.25	2.74 ± 0.82	4.44 ± 1.49	10.59 ± 3.25	7.32 ± 2.39
	-1.18 ± 0.28	-1.39 ± 0.28	-0.85 ± 0.32	-1.18 ± 0.28	-1.08 ± 0.34	-1.40 ± 0.26	-0.91 ± 0.34	-1.16 ± 0.32	-1.45 ± 0.26	-1.22 ± 0.27
O	7.32 ± 2.39	5.87 ± 1.96	1.63 ± 0.28	7.73 ± 2.50	3.56 ± 1.16	11.15 ± 3.38	2.74 ± 0.82	3.37 ± 1.09	8.15 ± 2.62	9.55 ± 2.99
	-1.17 ± 0.27	-1.39 ± 0.28	-0.69 ± 0.27	-1.23 ± 0.28	-1.08 ± 0.34	–	-0.91 ± 0.34	-1.00 ± 0.34	-1.29 ± 0.30	-1.33 ± 0.31
P	7.73 ± 2.50	7.73 ± 2.50	1.43 ± 0.20	7.73 ± 2.50	3.76 ± 1.24	8.60 ± 2.74	3.56 ± 1.16	4.44 ± 1.49	8.15 ± 2.62	7.32 ± 2.39
	-1.18 ± 0.28	-1.43 ± 0.28	-0.69 ± 0.25	-1.28 ± 0.28	-1.30 ± 0.34	-1.45 ± 0.32	-1.03 ± 0.34	-1.11 ± 0.32	–	-1.22 ± 0.27

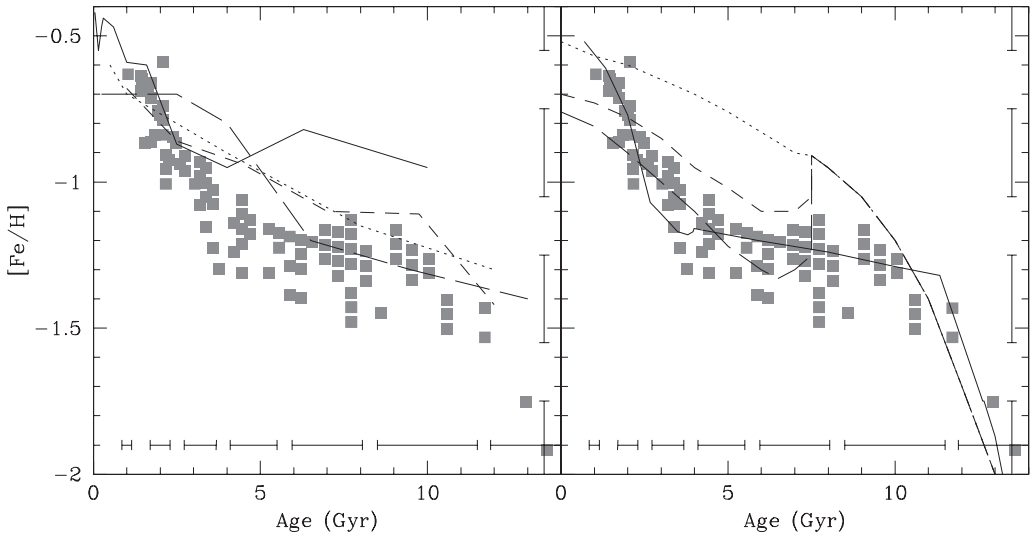

Figure 6. AMR for the presently studied SMC star fields (grey boxes), with typical age and metallicity error bars drawn at the margins. Left-hand panel: the AMRs by HZ04 (solid line), Dolphin et al. (2001, long-dashed line), Carrera et al. (2008, short-dashed line) and NAGHCM (dotted line) are overplotted. Right-hand panel: the modelled AMRs by PT98 (solid line) and TB10 (dotted, short-dashed and long-dashed lines) are superimposed. The three curves correspond to mergers with the mass ratio of 1–4 (long-dashed curve), to an equal-mass merger (short-dashed curve) and to a no-merger event (dotted curve), respectively.

technique. From them, a star field AMR was derived independent of any previous approach.

(ii) Star fields do not possess gradients in age and metallicity, and stellar populations formed since ∼2 Gyr ago are more metal rich than [Fe/H] ~ -0.8 dex and are confined to the innermost region (semi-major axis $\lesssim 1^\circ$).

(iii) We found that a comprehensive picture of the star field AMR is also composed of two enhanced formation processes: the most

© 2012 The Author, MNRAS **422,** 1109–1121
Monthly Notices of the Royal Astronomical Society © 2012 RAS

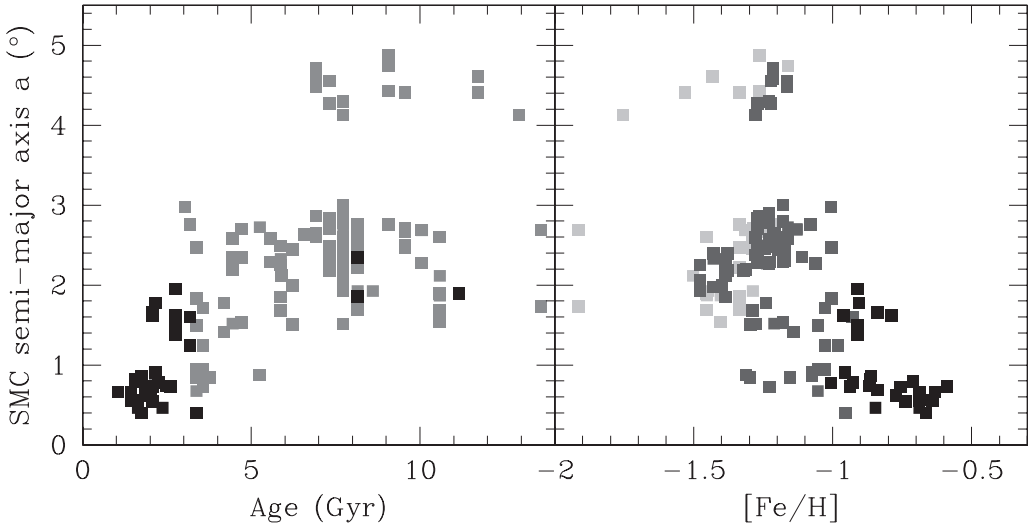

Figure 7. Relationships between the SMC semi-major axis and the star field ages (left-hand panel) and metallicities (right-hand panel) for the studied SMC fields. See the text for details about the colour-coded boxes.

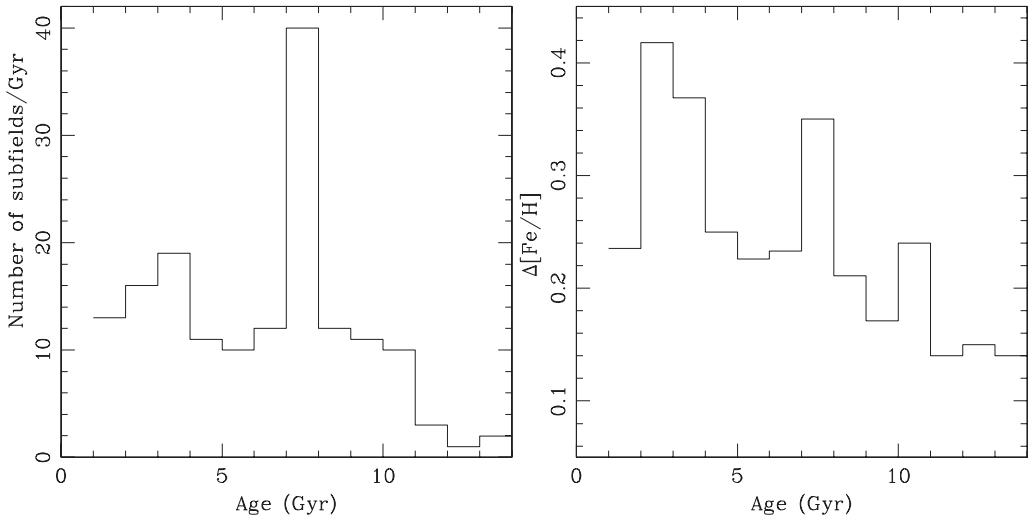

Figure 8. The age distribution (left-hand panel) and the metallicity spread as a function of age (right-hand panel) of the studied SMC fields.

recent peaked at an age of ∼2 Gyr, and an earlier one detected at an age of ∼7.5 Gyr. These features, also seen in the cluster AMR, allows us to conclude that both field and cluster populations share similar chemical evolution histories.

ACKNOWLEDGMENTS

I greatly appreciate the comments and suggestions raised by the reviewer which helped me to improve the manuscript. I also thank Owain Snaith for a careful reading of the manuscript. This research draws upon data as distributed by the NOAO Science Archive. NOAO is operated by the Association of Universities for Research in Astronomy (AURA), Inc., under a cooperative agreement with the National Science Foundation. This work was partially supported by the Argentinean institutions CONICET and Agencia Nacional de Promoción Científica y Tecnológica (ANPCyT).

REFERENCES

Burstein D., Heiles C., 1982, AJ, 87, 1165
Canterna R., 1976, AJ, 81, 228
Carrera R., Gallart C., Aparicio A., Costa E., Méndez R. A., Noël N. E. D., 2008, AJ, 136, 1039
Chiosi E., Vallenari A., 2007, A&A, 466, 165
Cignoni M. et al., 2009, AJ, 137, 3668
Crowl H. H., Sarajedini A., Piatti A. E., Geisler D., Bica E., Clariá J. J., Santos J. F. C., Jr, 2001, AJ, 122, 220
Da Costa G. S., Armandroff T. E., 1990, AJ, 100, 162
Dolphin A. E., Walker A. R., Hodge P. W., Mateo M., Olszewski E. W., Schommer R. A., Suntzeff N. B., 2001, ApJ, 562, 303
Geisler D., 1996, AJ, 111, 480
Geisler D., Sarajedini A., 1999, AJ, 117, 308
Geisler D., Bica E., Dottori H., Clariá J. J., Piatti A. E., Santos J. F. C., Jr, 1997, AJ, 114, 1920
Geisler D., Piatti A. E., Bica E., Clariá J. J., 2003, MNRAS, 341, 771

Girardi L., Bertelli G., Bressan A., Chiosi C., Groenewegen M. A. T., Marigo P., Salasnich B., Weiss A., 2002, A&A, 391, 195
Glatt K., Grebel E. K., Koch A., 2010, A&A, 517, 50
Harris J., Zaritsky D., 2004, AJ, 127, 1531 (HZ04)
Harris J., Zaritsky D., 2009, AJ, 138, 1243
McCumber M. P., Garnett D. R., Dufour R. J., 2005, AJ, 130, 1083
Noël N. E. D., Aparicio A., Gallart C., Hidalgo S. L., Costa E., Méndez R. A., 2009, ApJ, 705, 1260 (NAGHCM)
Olsen K. A. G., Salyk C., 2002, AJ, 124, 2045
Paczynski B., Stanek K. Z., 1998, ApJ, 494, L219
Pagel B. E. J., Tautvaišienė G., 1998, MNRAS, 299, 535 (PT98)
Parisi M. C., Grocholski A. J., Geisler D., Sarajedini A., Clariá J. J., 2009, AJ, 138, 517
Piatti A. E., 2011a, MNRAS, 418, L69
Piatti A. E., 2011b, MNRAS, 416, L89
Piatti A. E., Geisler D., Bica E., Clariá J. J., 2003a, MNRAS, 343, 851
Piatti A. E., Bica E., Geisler D., Clariá J. J., 2003b, MNRAS, 344, 965
Piatti A. E., Santos J. F. C., Jr, Clariá, Bica E., Ahumada A. V., Parisi M. C., 2005, A&A, 440, 111
Piatti A. E., Sarajedini A., Geisler D., Clark D., Seguel J., 2007, MNRAS, 377, 300
Piatti A. E., Geisler D., Sarajedini A., Gallart C., Wischnjewsky M., 2008, MNRAS, 389, 429
Piatti A. E., Clariá J. J., Bica E., Geisler D., Ahumada A. V., Girardi L., 2011, MNRAS, 417, 1559
Sabbi E. et al., 2009, ApJ, 703, 721
Stetson P. B., Davis L. E., Crabtree D. R., 1990, in Jacoby G. H., ed. ASP Conf. Ser. Vol. 8, CCDs in Astronomy. Astron. Soc. Pac., San Francisco, p. 289
Subramaniam A., 2003, ApJ, 598, L19
Tsujimoto T., Bekki K., 2010, ApJ, 700, L69

This paper has been typeset from a TEX/LATEX file prepared by the author.